

7.4. THEORETICAL DIFFUSER PERFORMANCE

7.4.1. General Considerations in Diffuser Analysis

A diffuser is an expanding duct. The primary objective of a diffuser is to recover fluid static pressure from a fluid stream while reducing the flow velocity. The fluid slows as it passes through a diffuser, and a portion of the kinetic energy of the flow is converted into the potential energy of pressure. An efficient diffuser is one which converts the highest possible percentage of kinetic energy into pressure within a given restriction on diffuser length or expansion ratio.

In a diffuser, the pressure gradient opposes the flow (Table 7-2). As a result, the boundary layer in a diffuser decelerates and thickens rapidly, and it can separate from the diffuser walls to form large unsteady eddies that block the diffuser flow (Ref. 7-25). The separation of flow from the diffuser walls is called diffuser stall, and it virtually always degrades the diffuser pressure recovery. Thus, the limit of diffuser performance is largely governed by boundary layer growth and the onset of stall.

7.4.2. Theoretical Aspects of Diffuser Performance

Consider the control volume of Fig. 7-6, which is bounded by the interior walls of the diffuser. The flow is steady and incompressible. Conservation of mass for this control volume is given by frame 4 of Table 5-1 with constant density, $\rho_1 = \rho_2 = \rho = \text{constant}$,

$$U_1 A_1 = U_2 A_2, \quad (7-39)$$

where the average velocities

$$U = \frac{1}{A} \int_A u \, dA \quad (7-40)$$

are averages of the axial velocity over the diffuser cross section A. Conservation of energy for this control volume

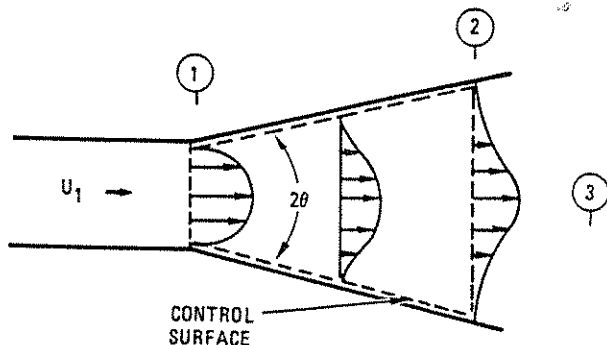


Fig. 7-6. Control surface for a diffuser with a free discharge. The boundary layer is retarded at the diffuser walls. U_1 is the average inlet velocity.

is described by frame 5 of Table 5-2 with the heat transfer and shaft work terms set to zero ($\dot{W} = \dot{Q} = 0$):

$$\begin{aligned} \rho \int_{A_1} \left(u + \frac{p}{\rho} + \frac{u^2}{2} \right) \vec{u} \cdot \hat{n} \, dA \\ = \rho \int_{A_2} \left(u + \frac{p}{\rho} + \frac{u^2}{2} \right) \vec{u} \cdot \hat{n} \, dA. \end{aligned} \quad (7-41)$$

\vec{u} is the local velocity vector, which has magnitude u . \hat{n} is the unit outward normal from the control surface. If (1) the changes in internal energy u are neglected (that is, viscous dissipation is neglected), (2) the static pressure p is uniform over each diffuser cross section of area A (as corresponds to experimental observation, Ref. 7-26), and (3) attention is restricted to components of flow parallel to the centerline of the diffuser, then the integrals of Eq. (7-41) may be considerably simplified:

$$p_1 \int_{A_1} u \, dA + \frac{\rho}{2} \int_{A_1} u^3 \, dA = p_2 \int_{A_2} u \, dA + \frac{\rho}{2} \int_{A_2} u^3 \, dA, \quad (7-42)$$

since the only nonzero terms are integrals over the areas A_1 and A_2 (Fig. 7-6). The axial flow velocity u will vary from zero at the diffuser walls to a peak value along the diffuser centerline. This velocity distribution is characterized by a kinetic energy flux profile factor,

$$\alpha = \frac{1}{A} \int_A \left(\frac{u}{U} \right)^3 \, dA, \quad (7-43)$$

which will generally vary along the diffuser axis. α is the ratio of the transport of fluid kinetic energy passing through the diffuser cross section of area A to the minimum possible transport of fluid kinetic energy at the same mass flow. The minimum value of the kinetic energy flux profile factor is $\alpha = 1$, which corresponds to uniform flow. α increases as the flow becomes peaked. If the peak of the exit flow from a diffuser is minimized (α_{exit} is minimum), the kinetic energy exiting the diffuser is minimized and, by conservation of energy, the pressure recovery is maximized. Thus, a uniform exit flow produces the best pressure recovery in any diffuser.

By incorporating Eqs. (7-39), (7-40), and (7-43) into Eq. (7-42) and rearranging, the nondimensionalized static pressure rise through the diffuser is predicted in terms of the area ratio ($A_2/A_1 > 1$) and the kinetic energy flux profile factors:

$$\frac{p_2 - p_1}{\frac{1}{2} \rho U_1^2} \Big|_{\text{ideal non-uniform flow}} = \alpha_1 - \alpha_2 \left(\frac{A_1}{A_2} \right)^2. \quad (7-44)$$

The diffuser pressure recovery is strongly influenced by the flow profile at the entrance and exit through the profile parameter α . For uniform flow profiles, $u = U$ and $\alpha_1 = \alpha_2 = 1$, and this equation becomes

$$\left. \frac{p_2 - p_1}{\frac{1}{2}\rho U_1^2} \right|_{\text{ideal uniform flow}} = 1 - \left(\frac{A_1}{A_2} \right)^2. \quad (7-45)$$

Since the diffuser is an expanding duct, A_2/A_1 exceeds 1.0 and the pressure will rise through the diffuser as the velocity falls, although viscous dissipation will diminish the pressure rise from that predicted by these equations.

Equation (7-44) implies that the pressure recovery through a diffuser is maximized by increasing α_1 , hence increasing the peakedness of the inlet profile, and by minimizing α_2 , hence making the outlet flow as uniform as possible. Unfortunately, the common situation is just the opposite. Viscous friction at the diffuser walls peaks the exit profile and increases α_2 over α_1 .

The extreme example of a peaked exit flow profile is jet flow. If the flow separates from the diffuser walls near the throat and maintains a uniform narrow jet through the diffuser, it can be easily shown from Eq. (7-43) that for a uniform jet of velocity U_1 over area A_1 ,

$$\alpha_1 = 1, \quad \alpha_2 = (A_2/A_1)^2.$$

The corresponding pressure recovery is zero, with $p_1 = p_2$ [Eq. (7-44)]. Jet flow reduces the diffuser efficiency to zero, which demonstrates that diffuser effectiveness is largely governed by the degree to which the flow conforms to the diffuser walls.

7.4.3. Diffuser Stall

Diffuser stall is the separation of flow from the diffuser walls and the formation of appreciable regions of unsteady separated flow within the diffuser. Diffuser stall can be delineated into regimes as illustrated in Table 7-6 for two-dimensional diffusers with straight walls. Both the profile of flow exiting from the diffuser and the diffuser pressure recovery are intimately related to the presence of diffuser stall. Stalled regions of separated fluid can block the diffuser flow, and they often result in severe asymmetry and unsteadiness of the exit flow. This tendency of diffusers to stall generally makes the diffuser the least stable component in a fluid circuit.

Diffuser stall is a function of (1) the diffuser inlet conditions, (2) the diffuser exit conditions, (3) the Reynolds number, (4) the Mach number, and, most important, (5) the diffuser geometry (Refs. 7-27 through 7-38). Over wide ranges of turbulent flow (Reynolds number, based on inlet flow velocity and inlet diameter, in excess of 5×10^4), the stall characteristics are primarily a function of diffuser geometry (Ref. 7-27). Regimes of diffuser flow are given as functions of diffuser geometry in Fig. 7-7(a) for two-dimensional diffusers and in Fig. 7-8 for conical and annular diffusers. These stall regimes are not as distinct as implied by Table 7-6 and Fig. 7-7(a), but rather blend into one another. Note that the geometry of the two-dimensional diffuser, shown in Fig. 7-9, can be specified either by the diffuser angle θ and the divergence ratio N/W_1 or by the area ratio A_2/H_1 and the divergence ratio N/W_1 . Lines of first appreciable stall are given in Fig. 7-8(b) for conical and annular diffusers. The higher

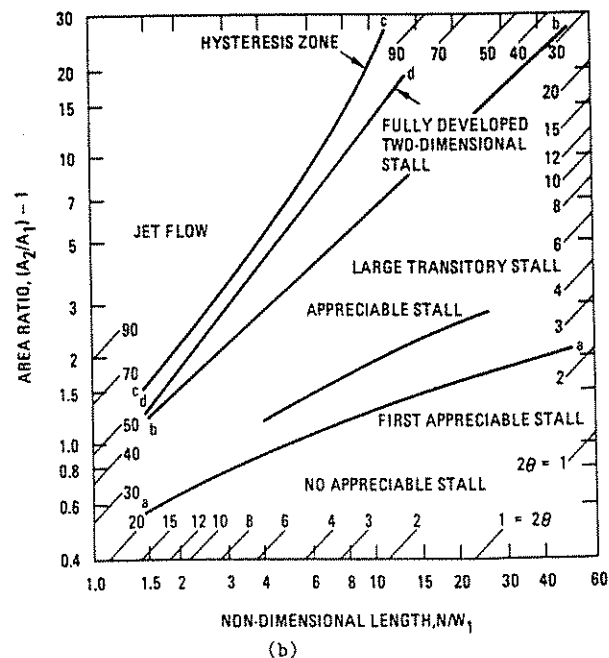
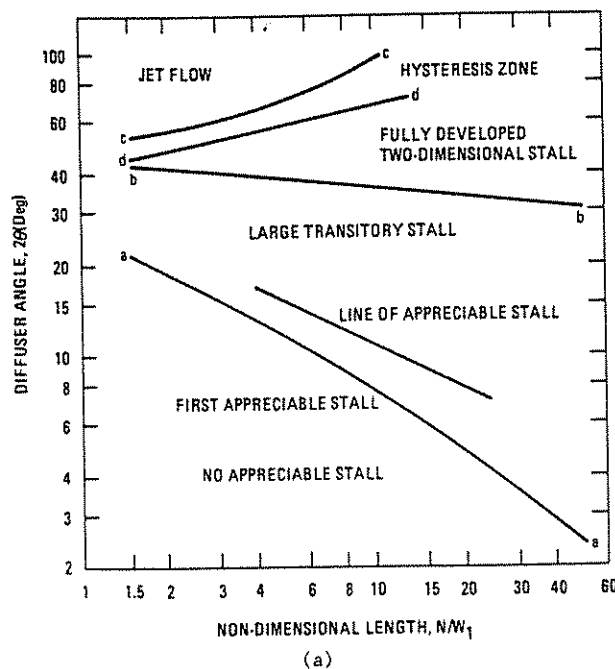
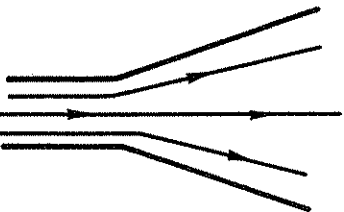
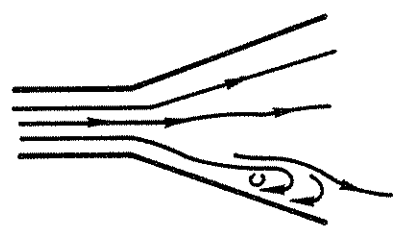
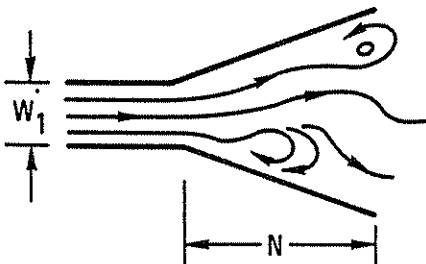
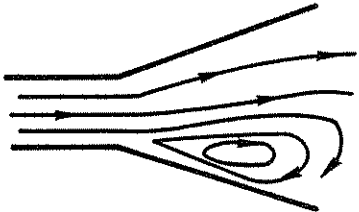
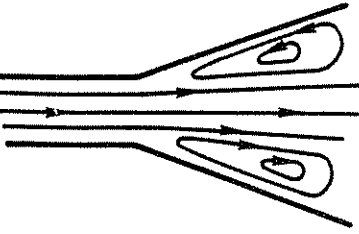
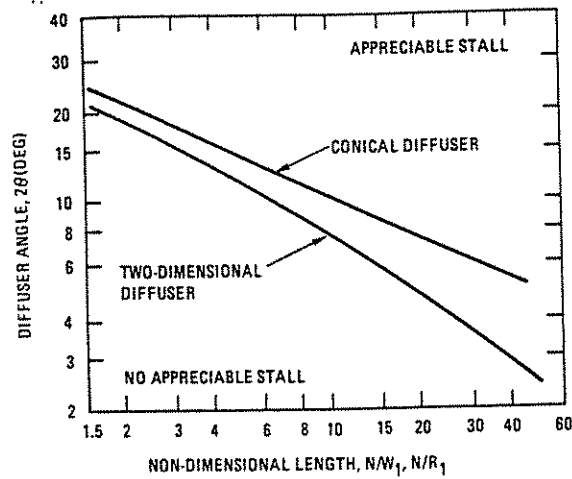


Fig. 7-7. Stall regimes for two-dimensional straight-walled diffusers. In the hysteresis zone, the flow varies between jet flow and fully developed stall. Graphs (a) and (b) are equivalent. See Fig. 7-9 and Table 7-6 for definition of terms. (Refs. 7-27, 7-29, 7-36.)

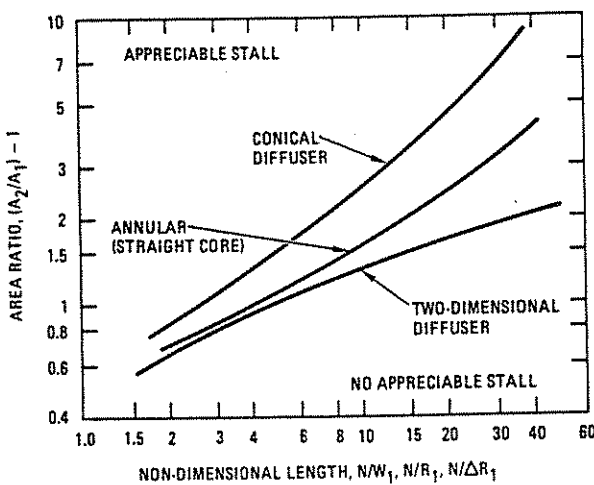
Table 7-6. Definition of Diffuser Stall Regimes.

These stall regimes apply to two-dimensional diffusers (two parallel walls and two diverging walls, Fig. 7-9. It is reasonable to believe that they apply to other diffusers. The divergence angle is exaggerated. Also see Fig. 7-7. (Refs. 7-27 through 7-29.)

Description	Characteristics
<p>1. Unstalled</p> 	<p>Flow follows diffuser contours. Flow is steady.</p>
<p>2. Appreciable Stall</p> 	<p>Flow generally follows diffuser contours. Boundary layers thicken. Small regions of separation and erratic flow are generally first seen in corners and they occupy no more than 1/5 of diffuser wall. There is little or no reverse flow.</p>
<p>3. Large Transitory Stall</p> 	<p>Flow is erratic with gross oscillation of pressure and overall flow pattern. Stalled regions with reverse flow form and then wash out.</p> <p>$N/W_1 < 4$: stalls occur on 1 diverging wall.</p> <p>$4 < N/W_1 < 12$: stalls occur on both diverging walls (shown).</p> <p>$N/W_1 > 16$: stalls occur on parallel walls..</p>
<p>4. Fully Developed Stall</p> 	<p>Flow separates near throat and forms a large, stable, fixed eddy along one diverging wall while the flow follows second diverging wall. Near-steady flow with reverse flow in eddy. Eddy can be moved from one wall to the other wall only by large disturbances.</p>
<p>5. Jet Flow</p> 	<p>Incoming flow separates from both diffuser walls near throat and proceeds as a jet down diffuser. Large fixed eddies form on diverging walls. Flow is steady with substantial regions of reverse flow. Diffuser pressure recovery is very poor.</p>



(a)



(b)

Fig. 7-8. Lines of first appreciable stall for two-dimensional, conical, and annular diffusers. The two graphs are equivalent. See Table 7-6 and Fig. 7-9 for definition of terms. (Refs. 7-29, 7-34, 7-37.)

onset of first stall in conical and annular diffusers compared with two-dimensional diffusers may be explained by the fact that stall often occurs first in the corners of two-dimensional diffusers, while conical and annular diffusers, being free of corners, are somewhat more resistant to stall (Refs. 7-29, 7-34). Complete stall regime maps are not available for conical and annular diffusers.

Turbulence in the flow and variations in the inlet flow profile can influence the stall and performance of a diffuser. High turbulence levels generally raise the line of appreciable stall (Fig. 7-7), thereby making the diffuser less prone to large transitory stall (Refs. 7-30, 7-36) and therefore capable of increased pressure recovery (Ref. 7-63). Increasing the boundary layer thickness or skewing the inlet flow profile lowers the line of first stall (Fig. 7-7), thereby making the diffuser more prone to stall and

capable of less pressure recovery, although this effect is generally small (Refs. 7-27, 7-35, 7-38).

Within the transitory stall regime, the eddies associated with stall will be formed and subsequently washed out in quasi-periodic fashion. The time for one cycle of this event varies about a typical mean period. For two-dimensional diffusers, the mean stall period (average time between events) can be predicted as follows (Ref. 7-33):

$$T_N = \alpha \frac{L \sin 2\theta}{U_1}, \quad (7-46)$$

where 2θ is the diffuser included angle, U_1 is the average entrance velocity, and L is the length of a diffuser side (Fig. 7-9). The dimensionless coefficient α is a function of the inlet Reynolds number (Ref. 7-39):

$$\alpha = (0.1 \pm 0.04) (U_1 W_1 / \nu)^{0.825}, \quad (7-47)$$

which agrees with experimental data obtained in water at $Re_1 = 7.5 \times 10^3$ ($\alpha = 180 \pm 60$, Ref. 7-33) and in air at $Re_1 = 3.7 \times 10^5$ ($\alpha = 4000 \pm 1500$, Ref. 7-39). The mean stall period is a valid estimate of the average period of 100 or more stall-washout events. Individual events can vary from $\frac{1}{2}T_N$ to $2T_N$ or more (Ref. 7-33). Additional discussion of periodic diffuser phenomena can be found in Refs. 7-31, 7-33, 7-39, 7-40, and 7-41.

Figure 7-10 shows the typical shape of pressure recovery as the diffuser angle is increased. The maximum pressure recovery occurs slightly above the line of first appreciable stall for two-dimensional diffusers and slightly below this line for conical and annular diffusers. The formation of large transitory or fixed stall significantly degrades the pressure recovery. For the same divergence angle, the pressure recovery is higher in diffusers which contain transitory stall than in diffusers in which a large fixed stall has developed (Ref. 7-27).

7.5. DIFFUSER PRESSURE RECOVERY COEFFICIENT

7.5.1. General Considerations

The actual recovery of static pressure for flow through a diffuser can be specified by an experimentally determined static pressure recovery coefficient:

$$C_p = \frac{p_2 - p_1}{\frac{1}{2} \rho U_1^2}. \quad (7-48)$$

p_1 and p_2 are the static pressures at the diffuser inlet and exhaust, respectively. ρ is the constant fluid density, and U_1 is the average flow velocity through the diffuser inlet (Fig. 7-6). Consistent sets of units are given in Table 3-1.

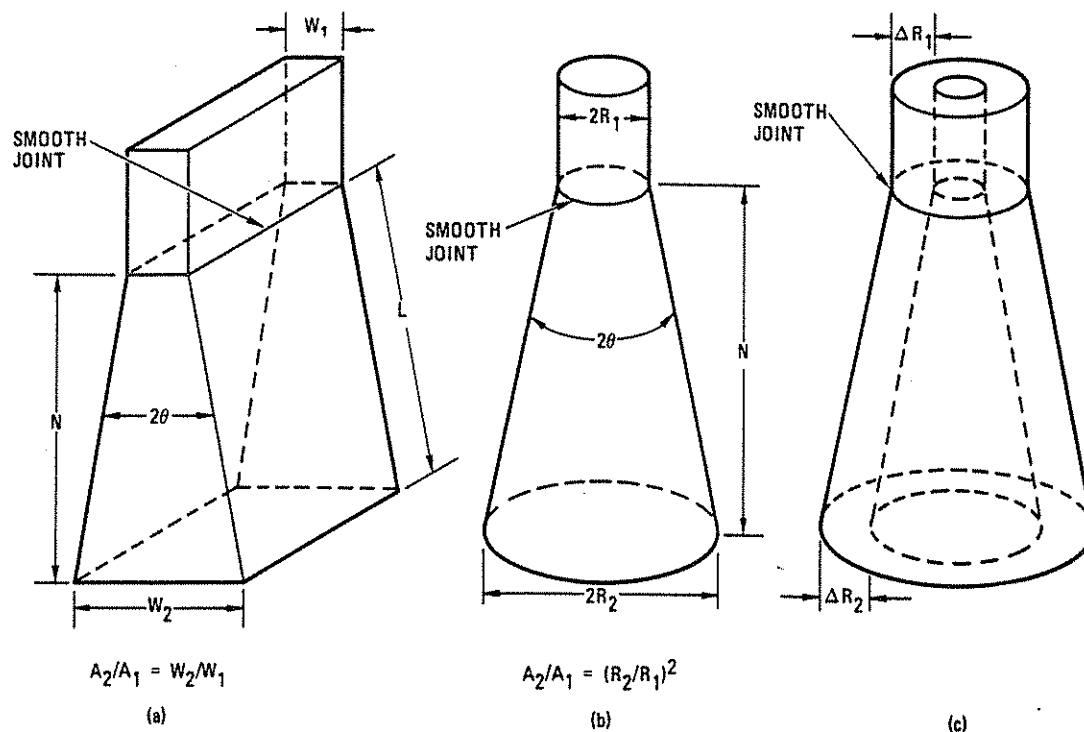


Fig. 7-9. Two-dimensional (a), conical (b), and annular (c) straight-walled diffusers. 2θ is the included diffuser angle.

(Note that this C_p is not identical to the same symbol used previously in this chapter for the specific heat at constant pressure.) For uniform entrance and exit flow and no friction losses, the ideal static pressure recovery coefficient can be deduced from Eq. (7-45),

$$C_p|_{\text{ideal uniform flow}} = 1 - \left(\frac{A_1}{A_2}\right)^2, \quad (7-49)$$

where A_1 and A_2 are the entrance and exit flow areas, respectively. Using Eqs. (7-48) and (7-49), a diffuser effectiveness can be defined to measure the actual diffuser

performance against the theoretical ideal:

$$\eta = \frac{\text{Actual Static Pressure Recovery}}{\text{Ideal Static Pressure Recovery}} = \frac{C_p}{1 - (A_1/A_2)^2}. \quad (7-50)$$

In practice, C_p will generally fall below the theoretical ideal and η will be less than 1.0. Viscous dissipation and velocity peaking in the outlet stream reduce the pressure recovery. There will be an additional loss of kinetic energy of the exiting stream for a diffuser which discharges into a large reservoir of still fluid. It is possible, however, for C_p to exceed the ideal value and η to exceed 1.0 if the inlet stream is highly peaked and the exit stream is nearly uniform (see Section 7.4.2).

A total pressure loss coefficient K for a diffuser can be defined by the change in total pressure through the diffuser:

$$p_1 + \frac{1}{2} \rho U_1^2 - \left(p_2 + \frac{1}{2} \rho U_2^2 \right) = \frac{1}{2} \rho U_1^2 K. \quad (7-51)$$

Using Eqs. (7-39) and (7-48), the loss coefficient K and the pressure recovery coefficient C_p are related by

$$K = 1 - (A_1/A_2)^2 - C_p, \quad (7-52)$$

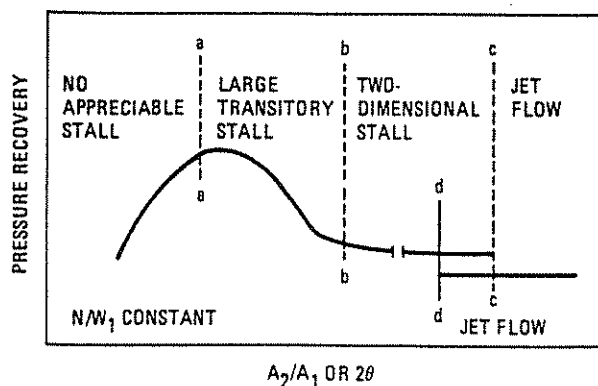


Fig. 7-10. Relationship between flow regimes and pressure recovery for a two-dimensional diffuser (Ref. 7-27). The lines correspond to stall regimes of Fig. 7-7(a).

and for a diffuser with a free discharge into a large reservoir, $A_2 = \infty$ and

$$K = 1 - C_p \quad (7-53)$$

For a perfect diffuser, $C_p = 1$ and $K = 0$.

Ordinarily, one is constrained in diffuser design by the overall length or area ratio. The two dashed lines in Fig. 7-11 represent solutions to two common design problems:

C_p^* = Locus of points which define the diffuser area ratios producing the maximum static pressure recovery in a given nondimensional length. (Given the ratio of overall length to inlet width, what ratio of outlet to inlet area produces the maximum static pressure recovery?)

C_p^* = Locus of points which define the diffuser nondimensional length producing the maximum pressure recovery for a prescribed area ratio. (Given the ratio of outlet to inlet area, what ratio of overall length to inlet width produces the maximum static pressure recovery?)

C_p^* nearly always lies below C_p on a plot such as Fig. 7-11, and both lines generally lie at or near the range of onset of stall.

While notable progress has been made for analytically predicting diffuser performance (Refs. 7-42 through 7-47), computational predictions are hindered by the large amounts of computer time required on even the fastest machines and by inaccuracies in stall and post-stall phenomena which are present in many diffusers of practical importance.

The data in the following section are entirely the result of painstaking experiments on diffusers which discharge into large plenums (free discharge). This is the most common diffuser application. Relatively little data is available for diffusers which act solely as expansions between constant area pipes or ducts. However, the data presented in frame 18 of Table 6-7 apply to a conical diffusing expansion in a pipe line. These data can be interpreted in terms of a static pressure recovery coefficient by applying Eq. (7-52).

7.5.2. Performance of Diffusers with Free Discharge

Two-Dimensional Diffusers. Maps of the static pressure recovery coefficient C_p [Eq. (7-48)] for two-dimensional diffusers [Fig. 7-9(a)] with a free discharge are given in Fig. 7-11 for two inlet boundary layer thicknesses. C_p is generally a function of the diffuser geometry and inlet boundary layer profile, as indicated in Fig. 7-11, the inlet Reynolds number and flow profile, and the conditions at the diffuser exit, which for a free discharge is a

reservoir of static fluid. The performance generally decreases with increasing inlet boundary layer thickness, as indicated in Fig. 7-11 (Refs. 7-27, 7-35).

The two boundary layer thicknesses of Fig. 7-11 were obtained by varying the length of inlet ducting into the diffuser. The plane boundary layer displacement thickness is defined as

$$\delta_1 = \int_0^{w_1/2} \left(1 - \frac{u}{U_c} \right) dy, \quad (7-54)$$

where u is the local velocity at a distance y from the inlet duct wall and U_c is the centerline velocity. A thickness of $2\delta_1/W_1 \approx 0.1$ corresponds to a fully developed boundary layer in Fig. 7-11. Diffuser performance generally decreases with decreasing Reynolds number, which ordinarily corresponds to increasing boundary layer thickness. However, if the inlet Reynolds numbers are in excess of $Re = U_1 W_1/\nu = 5 \cdot 10^4$, then the inlet boundary layers are fully turbulent and performance becomes nearly independent of Reynolds number (Refs. 7-27, 7-48).

For an area ratio of $A_2/A_1 = 2$ and $N/W_1 = 8$, the decrease in performance with increasing inlet boundary thickness is as follows (Ref. 7-27):

$2\delta_1/W_1$	0.007	0.015	0.03	0.05
C_p	0.69	0.67	0.65	0.60

While this boundary layer influence is significant, it is generally less important to diffuser performance than the geometry of the diffuser.

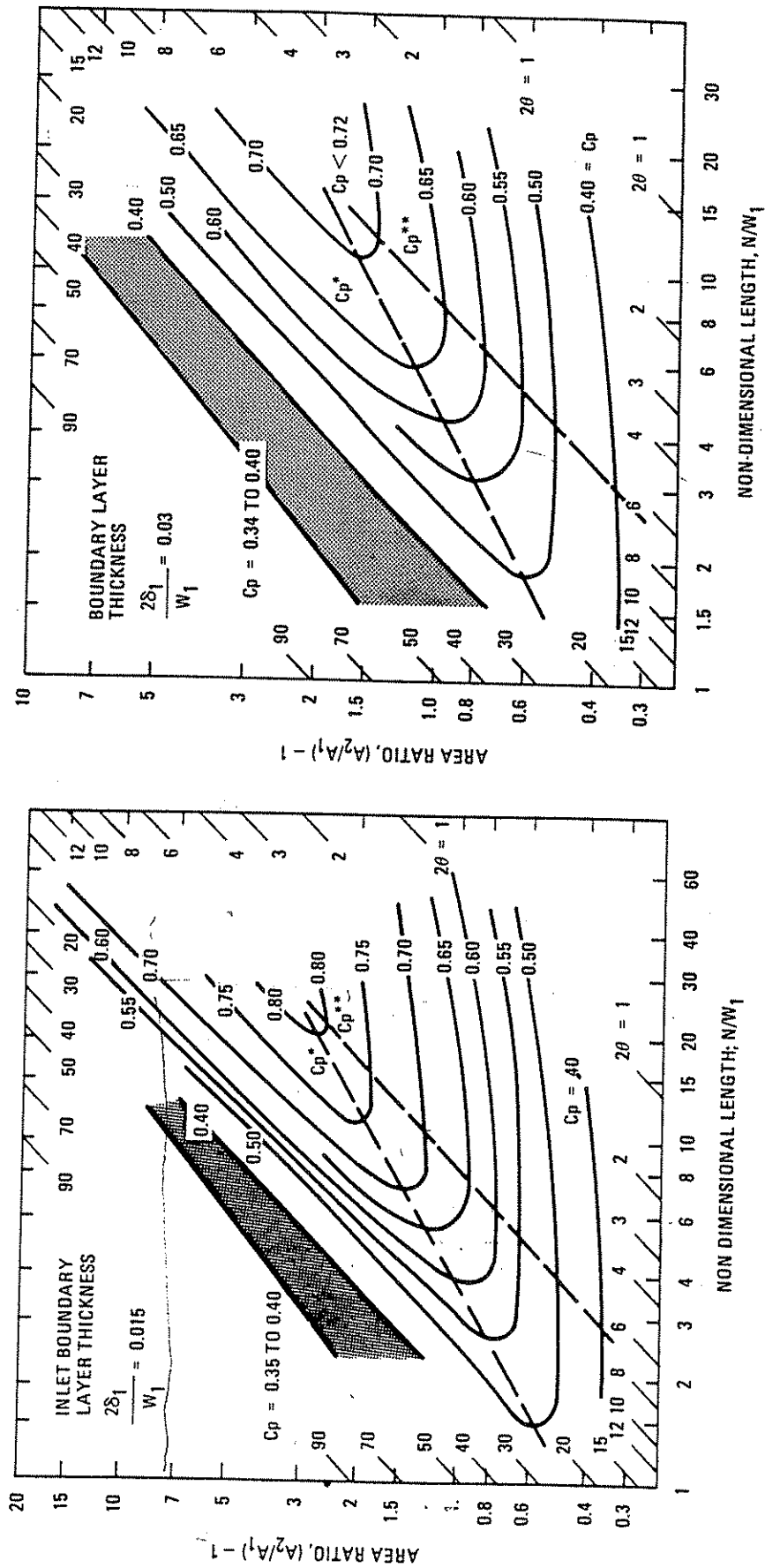
The geometry of a straight-walled, two-dimensional diffuser can be specified by the following parameters: nondimensional length, N/W_1 , and either included angle 2θ or area ratio A_2/A_1 . From the geometry of the diffuser [Fig. 7-9(a)], it can be shown that

$$\tan \theta = \frac{W_2 - W_1}{2N} = \frac{W_1}{2N} \left(\frac{W_2}{W_1} - 1 \right) = \frac{W_1}{2N} \left(\frac{A_2}{A_1} - 1 \right). \quad (7-55)$$

W_1 is the inlet width, W_2 is the outlet width, and N is the diffuser length. Taking the logarithm of this expression yields

$$\log_{10} (2 \tan \theta) = -\log_{10} \frac{N}{W_1} + \log_{10} \left(\frac{A_2}{A_1} - 1 \right). \quad (7-56)$$

Thus, lines of constant diffuser angle appear as straight, parallel, diagonal lines when plotted on a graph of \log_{10}



(a)

(b)

Fig. 7-11. Static pressure recovery coefficient C_p (Eq. 7-48) of straight-walled two-dimensional diffusers for two values of inlet boundary layer thickness. Inlet Reynolds number, $Re_1 = U_1 W_1 / \nu$, exceeds 5×10^4 . See Fig. 7-9(a) for definition of terms. (Ref. 7-27.)

(N/W_1) versus $\log_{10} [(A_2/A_1) - 1]$, as shown in Figs. 7-7(b) and 7-11.

The optimum line C_p^* (see Section 7.5.1) always lies below C_p on the plot of Fig. 7-11, and C_p^* is very nearly equal to a diffuser included angle of $2\theta \approx 7^\circ$, although the pressure contours are nearly level near C_p^* . The locations of C_p and C_p^* are nearly identical for the two boundary layer thicknesses of Figs. 7-11(a) and 7-11(b). Reneau and his co-workers have shown that for a range of inlet boundary layer thicknesses, the location of C_p is nearly independent of boundary layer thickness (Refs. 7-27, 7-26). This implies that the optimum diffuser geometry for a given nondimensional length can be chosen independently of the inlet boundary layer thickness for symmetric inlet flow. Inlet flow profiles which are skewed to one wall or are substantially nonuniform exhibit decreased performance compared with the nearly uniform profiles of Fig. 7-11, and their C_p optimal lines generally fall below those given in Fig. 7-11 (Ref. 7-38).

Comparing Fig. 7-7(b) and Fig. 7-11, it can be seen that both the C_p and C_p^* optimal lines lie within the range of appreciable stall. This implies that optimal two-dimensional diffusers will be marginally stable. Stability of a two-dimensional diffuser can be obtained only at the cost of a performance penalty by either (1) decreasing the diffuser angle or area ratio to place the diffuser well within the range of no appreciable stall, or (2) increasing diffuser angle or area ratio to the point where the diffuser lies well within the fixed stall or jet flow regime, or (3) vaning the diffuser. The first and third options require the smallest performance penalty.

Conical Diffusers. Maps of the static pressure recovery coefficient for a conical diffuser with a free discharge are given in Fig. 7-12 both as a function of area ratio A_2/A_1 and as a function of divergence angle 2θ . The relationship between these variables is obtained from the geometry of the diffuser [(Fig. 7-9(b))]:

$$\tan \theta = \frac{R_2 - R_1}{N_1} = \frac{R_1}{N} \left(\frac{R_2}{R_1} - 1 \right) = \frac{R_1}{N} \left[\left(\frac{A_2}{A_1} \right)^{1/2} - 1 \right]. \quad (7-57)$$

R_1 is the inlet radius, R_2 is the outlet radius, and N is the diffuser length. The inlet area is A_1 and A_2 is the outlet area. The static pressure recovery coefficient is generally a function of the diffuser geometry, as indicated in Fig. 7-12, the inlet Reynolds number, flow profile, and the conditions at the diffuser exit, which, for a free discharge, is a reservoir of static fluid. The pressure recovery generally decreases with increasing inlet boundary layer thickness. The data of Fig. 7-12 apply for thin inlet boundary layers, such as would develop over one or two diameters of a pipe having the same diameter as the

diffuser inlet. The data presented in Ref. 7-48 imply that the pressure recovery coefficients are 5–15% lower for thick inlet boundary layers such as would develop over long lengths of inlet pipe. Similarly, diffuser performance generally decreases with decreasing Reynolds number, which corresponds to increasing boundary layer thickness. However, if the inlet Reynolds number is in excess of $2U_1 R_1/\nu = 7 \times 10^4$, then the inlet boundary layer is fully turbulent and the performance will be substantially independent of Reynolds number (Ref. 7-34).

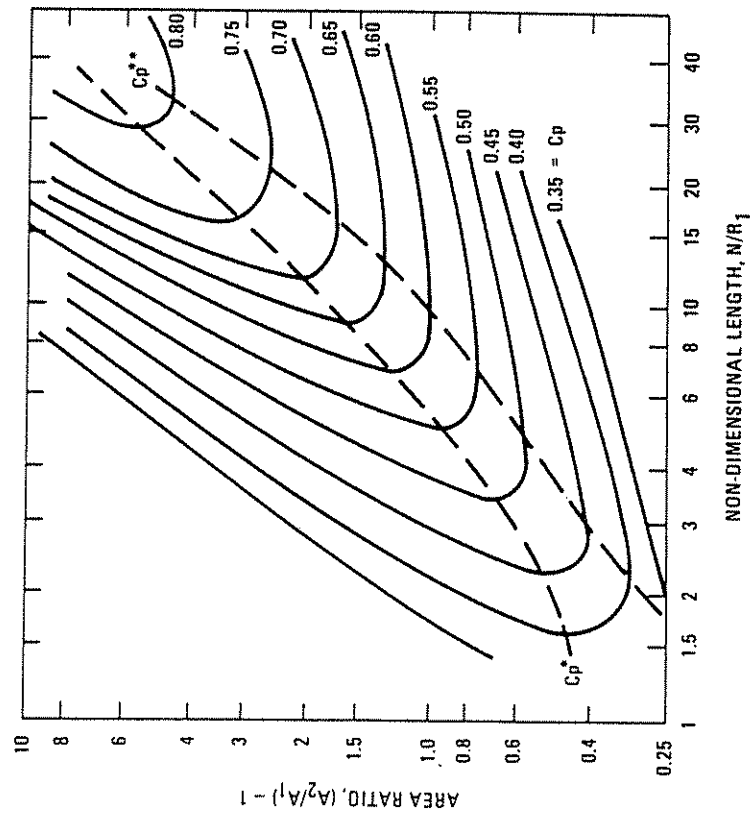
The optimal line C_p^* (see Section 7.5.1) always lies below C_p on the plots of Fig. 7-12, and C_p^* is very nearly equal to the diffuser included angle of $2\theta \approx 5^\circ$ (Ref. 7-26). Studies by Cockrell and Markland (Ref. 7-49) and by Sovran and Klomp (Ref. 7-26) and the data reported by Miller (Ref. 7-48, p. 168) indicate that the C_p optimum is nearly independent of the inlet boundary layer thickness. This implies that the C_p optimal diffuser geometry for a given nondimensional length can be chosen independently of boundary layer thickness for symmetric inlet boundary layers. The C_p^* optimal line may be influenced by boundary layer thickness, decreasing with increasing boundary layer thickness (Ref. 7-48, p. 168). Comparing Figs. 7-8 and 7-12, it can be seen that the optimal lines fall below the line of first appreciable stall, which implies that optimal conical diffusers will be stable and free of stall.

Swirl is defined as tangential rotation of the flow. Inlet swirl is often present in conical diffusers as a result of upstream rotating machinery. Experimental studies suggest that the effect of swirl on conical diffuser performance can be correlated with the stall regime. Inlet swirl has little effect on unstalled diffusers. However, swirl can substantially improve the performance of stalled diffusers and it produces a substantial upward shift in the optimal lines shown in Fig. 7-12 (Ref. 7-50). The swirl-induced performance improvement is apparently due to improved velocity distribution which yields a more uniform exit velocity profile (Ref. 7-51).

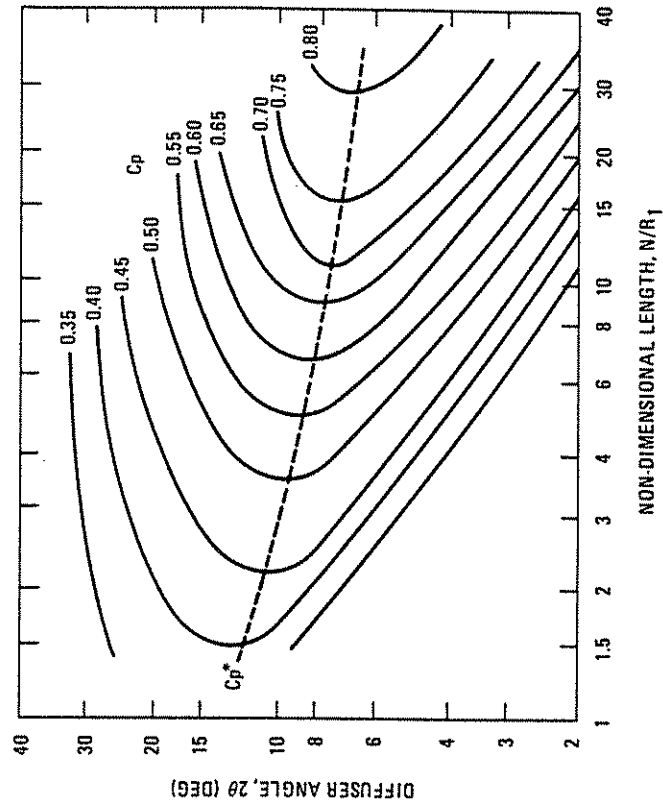
Annular Diffusers. A straight-walled annular diffuser is shown in Fig. 7-9(c) and in cross section in Fig. 7-13. A map of the static pressure recovery coefficient for an annular diffuser is given in Fig. 7-14 as a function of the area ratio A_2/A_1 and the nondimensional diffuser length $\bar{L}/\Delta R_1$. The average diffuser wall length and the inlet differential radius are defined as

$$\bar{L} = (L_i + L_o)/2, \quad \Delta R_1 = R_o - R_i. \quad (7-58)$$

L_i , L_o , R_o , and R_i are defined in Fig. 7-13. The annular diffuser geometry is by no means fixed by the two parameters $\bar{L}/\Delta R_1$ and A_2/A_1 . However, Sovran and Klomp (Ref. 7-26) have found that for common annular diffusers with wall angles in the 5° to 30° range and inlet



(a)



(b)

Fig. 7-12. Static pressure recovery coefficient C_p (Eq. 7-48) for conical diffusers with thin inlet boundary layer and inlet Reynolds number in excess of 75×10^3 . See Fig. 7-9(b) for geometry. (Ref. 7-34). Reproduced with permission.

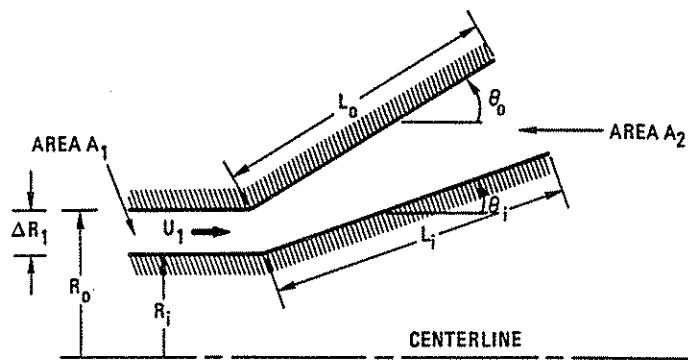


Fig. 7-13. Cross section of a straight-walled annular diffuser with a free discharge.

radius ratios of R_i/R_0 between 0.55 and 0.70, these two parameters correlate the majority of the experimental data. The inlet boundary layers for the data of Fig. 7-14 were relatively thin. The inlet Reynolds number varied over the range $4.8 \times 10^5 < U_1 \Delta R_1 / \nu < 8.5 \times 10^5$. It is reasonable to believe the static pressure recovery coefficient will be nearly independent of Reynolds number for $U_1 \Delta R_1 / \nu > 7 \times 10^4$ and that it will decrease slightly with thickening inlet boundary layers. Comparing Fig. 7-14 with Figs. 7-11(a) and 7-12(a), it can be seen that all three plots predict similar performance for two-dimensional variables of area ratio A_2/A_1 and nondimensional length.

The optimal line C_p^* lies below C_p (see Section 7.5.1). Based on the performance of two-dimensional and conical diffusers, it is reasonable to believe that the C_p line will be

nearly independent of the inlet boundary layer thickness. Comparing Fig. 7-8(b) with Fig. 7-14, it can be seen that the optimal annular diffusers generally lie below the line of first appreciable stall; this implies that optimal annular diffusers generally will be stable and free of stall.

One of the most common applications of annular diffusers is in the discharge of turbines. Studies of annular diffusers in turbomachinery outlets suggest that Fig. 7-14 provides a valid estimate of the diffuser performance with moderate swirl; a high degree of swirl may degrade the performance somewhat (Refs. 7-52, 7-53, 7-54).

Vaned Diffusers. The performance of short, wide-angle diffusers can often be considerably improved by the installation of vanes, as shown in Fig. 7-15. One to five

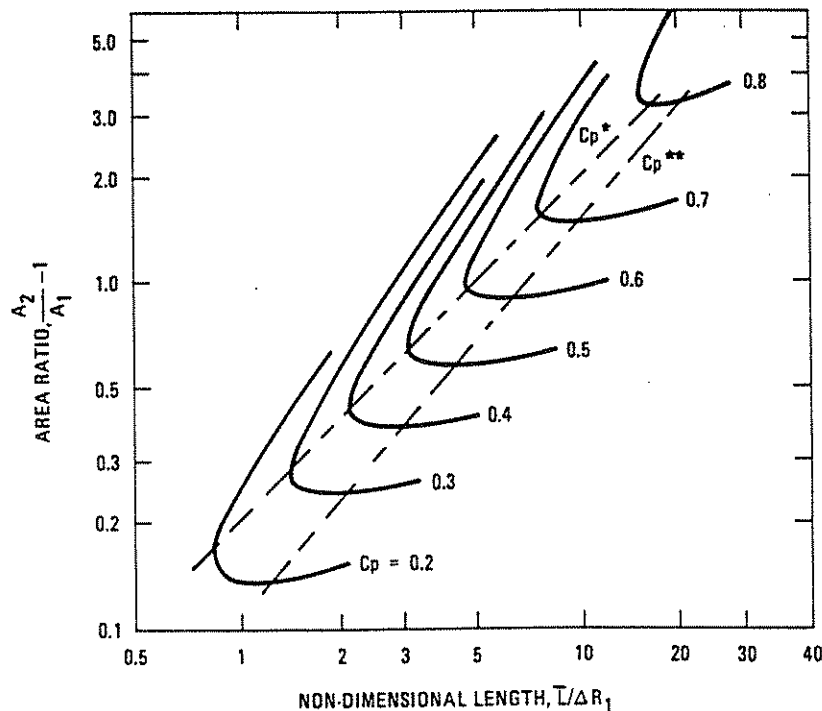


Fig. 7-14. Static pressure recovery coefficient for annular diffusers with thin inlet boundary layers in excess of $U_1 \Delta R_1 / \nu > 7 \times 10^4$. See Fig. 7-13 and Eq. (7-63) for definition in terms. (Ref. 7-26.) Reproduced with permission.

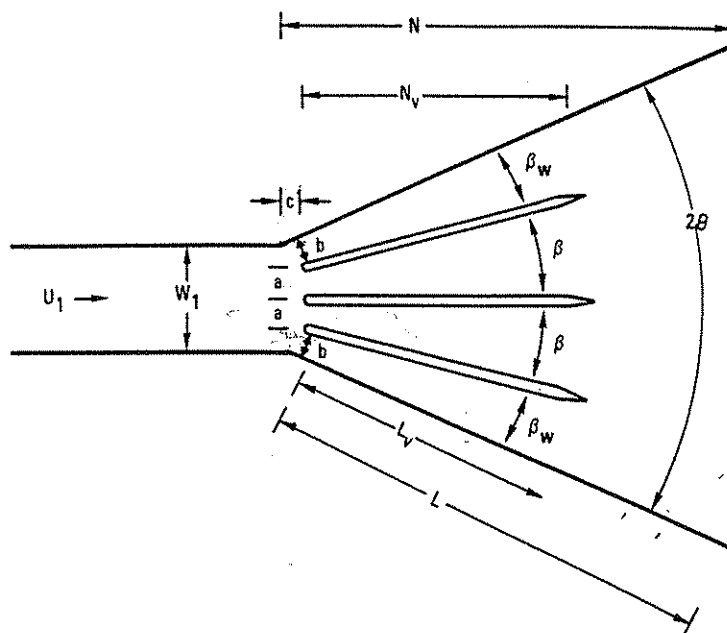


Fig. 7-15. A two-dimensional diffuser with three short vanes.

vanes have been installed in diffusers with included angles between 14° and 80° and area ratios as severe as 5 to 1. Vanes subdivide the diffuser into a series of diffusing passages, each of which will have divergence angles and area ratios much smaller than those of the vaneless diffuser. Thus, while the vaneless diffuser operates in the regime of stall or jet flow, the addition of vanes can produce a series of stall-free diffusing passages with each passage operating at near-optimum pressure recovery. The installation of vanes in badly stalled diffusers has been reported to (1) increase pressure recovery by as much as a factor of 2, (2) produce much steadier exit flow, and (3) yield uniform exit flow with as much as a factor of 2 reduction in the peak to average flow velocity (Ref. 7-55).

Successful vanes described in the literature generally follow the following design principles (Refs. 7-35, 7-36, 7-48, 7-55, 7-56):

1. The number of vanes is chosen so that the included angle of the passages between vanes is between 7° and 10° . That is, if n is the number of vanes, n is chosen so that

$$\beta = \frac{2\theta}{n+1} = 7^\circ \text{ to } 10^\circ. \quad (7-59)$$

2θ is the included angle of the diffuser (Fig. 7-15). The included angle of the wall passage is often slightly greater.

2. Equal spacing is used between the vanes. If a is the spacing between the leading edge of the vanes, measured perpendicular to the diffuser axis (Fig. 7-15),

$$a = W_1/(n+1). \quad (7-60)$$

3. While success has been obtained with vanes running the full length L of the diffuser, vanes as short as $0.25 < L_v/L < 0.6$ have yielded very good performance. The length of these shorter vanes is chosen so that the diffusing passage between vanes of included angle β and inlet width a operates at the maximum pressure recovery as indicated by either the C_p line (Fig. 7-11 for two-dimensional diffusers) or the line of appreciable stall (Fig. 7-7, provided the length is shorter than the diffuser length).

4. The leading edge of the vanes is set back slightly from the beginning of the diffuser divergence. This can be done by setting $1.0 < b \leq 1.2a$, or $W_1 < c < 0.15W_1$.
5. The vanes are straight. The leading edges of the vanes are rounded, and the trailing edges are tapered in at least a 5 to 1 taper to minimize exit losses. Vane thicknesses between $0.06W_1$ and $0.1W_1$ have been used. The thicker vanes require careful contouring of their leading and trailing edges.

Under these rules, the performance of the vaned diffuser can nearly equal that of the unvaned diffuser if the optimum, rather than the actual, divergence angle is used.

Feil (Ref. 7-56) offers the following improvements in the above rules for optimizing the performance of two-dimensional diffusers having curved leading edges, as shown in Fig. 7-16. The radius r is chosen so that

$$r = 3 W_1/4\theta. \quad (7-61)$$

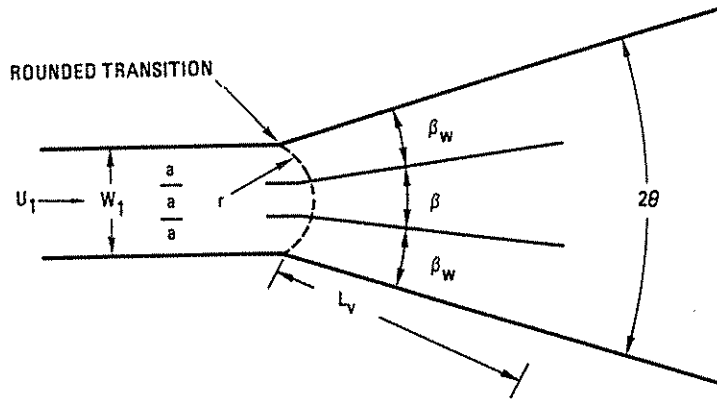


Fig. 7-16. Feil's vane system installed in a two-dimensional diffuser.

θ is here measured in radians. 2θ is the sum of the diffuser included angle and a correction angle which is dependent only on the diffuser area ratio:

$$2\theta = 2\theta_0 + 2\Delta\theta, \quad (7-62)$$

where $\Delta\theta$ in degrees is given below:

A_2/A_1	3.0	3.5	4.0	4.5	5.0
$\Delta\theta$ (deg)	4.5	6.0	6.7	7.3	7.5

The number of vanes is chosen so that

$$\beta = 2\theta/(n+1) \cong 7^\circ \text{ to } 10^\circ,$$

where n is the number of vanes. The spacing between vanes is $a = W_1/(n+1)$ (Fig. 7-16). The length of the vanes L_v is chosen as either 0.6 times the length of the diffuser side L or such that each diffusing passage operates at the line of appreciable stall as indicated in Fig. 7-7 for a two-dimensional diffuser, whichever is shorter.

While the rules presented in the previous two paragraphs were developed for two-dimensional diffusers, it is reasonable to believe, in the absence of contrary published data, that they can be applied directly to conical and annular diffusers.

Curved Wall Diffusers. Curved wall diffusers can be of two classes: (1) diffusers whose axis is straight but whose walls are curved in a bell or a trumpet shape, or (2) diffusers whose axis is curved so that the diffuser is the sum of a bend and a straight axis diffuser. Tests by Carlson et al. (Ref. 7-28) indicate that there is little advantage in utilizing a trumpet or bell wall shape over a straight wall in a straight axis, two-dimensional diffuser; moreover, the straight wall design is far easier to construct.

The losses in a curved axis diffuser (a diffusing bend) exceed those in a comparable straight axis diffuser. The

pressure recovery is lower, and the bending of the flow results in an exit maldistribution with higher flow velocities on the outside of the bend. However, a curved axis diffuser can be more efficient than the combination of a straight axis diffuser and a bend (Ref. 7-48). Considerable data on curved axis diffusers is presented in Refs. 7-29, 7-48, 7-57, and 7-58.

7.6. VENTURI TUBES

Venturi tubes are the union of a nozzle and a diffuser, as shown in Fig. 7-17. The purpose of a venturi tube is to create a region of low static pressure at the venturi throat which can be used to draw in a second fluid, as in a venturi carburetor, or to generate a pressure differential between the throat static pressure and the static pressure in the contiguous pipe line, as in a venturi flowmeter.

The mass flow rate through a venturi tube can be predicted by the same formulas for nozzles that are developed in Section 7.2. For incompressible flow, the mass flow rate is [Eq. (7-33)]

$$\dot{m} = C \frac{\pi d^2}{4} \left[\frac{1}{1 - (d/D)^4} \right]^{1/2} [2\rho(p_1 - p_2)]^{1/2}.$$

For compressible subsonic flow, the mass flow rate is [Eq. 7-36)]

$$\dot{m} = C \frac{\pi d^2}{4} \left[\frac{1}{1 - (d/D)^4} \right]^{1/2} [2\rho_1(p_1 - p_2)]^{1/2} Y.$$

C is the discharge coefficient, i.e., the ratio of the actual flow rate to the ideal flow rate for a given static pressure differential. p_1 is static pressure at the upstream tap where the diameter is D , and p_2 is the static pressure at the throat where the diameter is d . ρ is density and ρ_1 is the density at the upstream tap (see discussion at end of Section 7.2.3). Y is the expansion coefficient [Eq. (7-29), Table 7-3]. Consistent sets of units are given in Table 3-1.

Similarly, for the diffuser design,

$$p_0 - p_e = \frac{1}{2} \rho U^2 \left(1.5 + \frac{fL_1}{D} - C_p \right).$$

Comparing these two equations, it can be seen that the presence of the diffuser reduces the overall losses.

The mass flow through the cross duct is now easily computed from the above formula for the straight pipe design,

$$\dot{m} = \rho p U \frac{\pi D^2}{4} = \rho \frac{\pi D^2}{4} \left[\frac{2(p_0 - p_e)}{\rho} \right]^{1/2} / \left[1.5 + \frac{f(L_1 + L_2)}{D} \right]^{1/2},$$

and for the diffuser design,

$$\dot{m} = \rho \frac{U \pi D^2}{4} = \rho \frac{\pi D^2}{4} \left[\frac{2(p_0 - p_e)}{\rho} \right]^{1/2} / \left(1.5 + \frac{fL_1}{D} - C_p \right)^{1/2}.$$

These two expressions are evaluated for the parameters of Fig. 7-21 and the units of frame 7 of Table 3-1:

$$D = 6 \text{ in.}, \quad \rho = 1.91 \times 10^{-7} \text{ lb-sec}^2/\text{in.}^4,$$

$$L_1 = 96 \text{ in.}, \quad p_0 = 26 \text{ lb/in.}^2,$$

$$L_2 = 24 \text{ in.}, \quad p_e = 25 \text{ lb/in.}^2.$$

If the Reynolds number of the pipe flow is estimated initially as $Re = UD/\nu = 10^6$, where ν is kinematic viscosity, and the pipe is fully rough steel, then the surface roughness is $\epsilon \approx 0.002 \text{ in.}$ (Table 6-4), $\epsilon/D = 3.3 \times 10^{-4}$, and the friction factor is estimated from Fig. 6-8 to be

$$f = 0.016.$$

These parameters are sufficient to compute the flow rate through the straight pipe design:

$$U = 2400 \text{ in./sec (200 ft/sec)},$$

$$\dot{m} = 0.0130 \text{ lb-sec/in. (5.00 lb/sec)}.$$

For the diffuser design, the static pressure recovery coefficient must be found before the corresponding computation can be made. For an optimal conical diffuser of non-dimensional length $N/R_1 = 24 \text{ in.}/3$

in. = 6, Fig. 7-12(a) gives $C_p = 0.53$ at $(A_2/A_1) - 1 = 1.0$. This area ratio corresponds to $A_2/A_1 = 2.0$, $d/D = (2.0)^{1/2}$, or

$$d = (2.0)^{1/2} D = 8.48 \text{ in.}$$

In practice, the static pressure recovery coefficient will fall below $C_p = 0.53$ owing to the thick boundary layers in the present case, and so $C_p = 0.5$ will be used in the calculations. For $C_p = 0.5$, the velocity and mass flow through the diffuser design are

$$U = 2890 \text{ in./sec (240 ft/sec)},$$

$$\dot{m} = 0.015 \text{ lb-sec/in. (6.02 lb/sec)}.$$

Thus, by incorporating a diffuser, a 20% increase in flow rate is achieved over the straight pipe design for the same overall static pressure drop. An additional 20% improvement could be obtained by rounding the pipe inlet.

REFERENCES

- 7-1. Olson, A. T., "Nozzle Discharge Coefficients—Compressible Flow," *J. Fluids Eng.* 96, 21-24 (1974).
- 7-2. Weber, H. E., "Boundary Layer Calculation for Analysis and Design," *J. Fluids Eng.* 100, 232-236 (1978).
- 7-3. Keith, T. G., and J. E. A. John, "Calculated Orifice Plate Discharge Coefficients at Low Reynolds Numbers," *J. Fluids Eng.* 99, 424-425 (1977).
- 7-4. Cebeci, T., and P. Bradshaw, *Momentum Transfer in Boundary Layers* Hemisphere Publishing, Washington, D. C., 1977.
- 7-5. Benedict, R. P., and J. S. Wyler, "Analytical and Experimental Studies of ASME Flow Nozzles," *J. Fluids Eng.* 100, 265-275 (1978).
- 7-6. Cebeci, T., and A. M. O. Smith, *Analysis of Turbulent Boundary Layers*, Academic Press, New York, 1974.
- 7-7. Ashjaee, J., and J. P. Johnston, "Straight Walled, Two-Dimensional Diffusers—Transitory Stall and Peak Pressure Recovery," *J. Fluids Eng.* 102, 275-282 (1980).
- 7-8. Shapiro, A. H., *The Dynamics and Thermodynamics of Compressible Fluid Flow*, Vol. 1, Ronald Press, Inc., New York, 1953.
- 7-9. Hansen, A. G., *Fluid Mechanics*, John Wiley, New York, 1967.
- 7-10. Bean, H. S., (Ed.), *Fluid Meters, Their Theory and Application*, 6th Ed., The American Society of Mechanical Engineers, New York, 1971.
- 7-11. Head, V. P., "Improved Expansion Factors for Nozzles, Orifices and Variable-Area Meters," *J. Fluids Eng.* 96, 150-156 (1974).
- 7-12. Johnson, R. C., "Calculations of the Flow of Natural Gas through Critical Flow Nozzles," *J. Basic Eng.* 92, 580-589 (1970).
- 7-13. Jordan, D., and M. D. Mintz, *Air Tables*, McGraw-Hill, New York, 1965.
- 7-14. Leutheusser, H. J., "Flow Nozzles with Zero Beta Ratio," *J. Basic Eng.* 86, 538-542 (1964).
- 7-15. Alvi, S. H., et al., "Loss Characteristic of Orifices and Nozzles," *J. Fluids Eng.* 100, 299-307 (1978).
- 7-16. Miller, R. W., and O. Kneisel, "A Comparison Between Orifice and Flow Nozzle Laboratory Data and Published Coefficients," *J. Fluids Eng.* 96, 139-149 (1974). Also see R. W. Miller, "The

- Stolz and ASME-AGA Orifice Equations Compared to Laboratory Data," *J. Fluids Eng.* **101**, 483-490 (1979).
- 7-17. Benedict, R. P., "Loss Coefficients for Fluid Meters," *J. Fluids Eng.* **99**, 245-248 (1977).
- 7-18. International Organization for Standardization, "Measurement of Fluid Flow by Means of Orifice Plates, Nozzles and Venturi Tubes Inserted in Circular Cross Section Conduits Running Full," ISO Standard ISO No. 5167-1980(E), 1980.
- 7-19. Soundranayagam, S., "An Investigation Into the Performance of Two ISA Metering Nozzles of Finite and Zero Area Ratio," *J. Basic Eng.* **87**, 525-530 (1965).
- 7-20. Idel'chik, I. E., *Handbook of Hydraulic Resistance*, U.S. Department of Commerce, National Technical Information Service, Report AEC-TR-6630, 1960 (translated from Russian).
- 7-21. Harris, C. H., "Elimination of Hydraulic Eddy Current Loss at Intake," University of Washington Engineering Experimental Station, Bulletin No. 54, October 1930.
- 7-22. Grey, R. E., and H. D. Wilsted, "Performance of Conical Jet Nozzles in Terms of Flow and Velocity Coefficients," NACA Technical Note No. 1757, Lewis Flight Propulsion Laboratory, Cleveland, Ohio, 1948.
- 7-23. Freeman, J. R., "Experiments Relating to Hydraulics of Fire Streams," *Trans. ASCE* **21**, 303-482 (1888).
- 7-24. Rouse, H., et al., "Experimental Investigation of Fire Monitors on Nozzles," *Trans. ASCE* **117**, 1147-1188 (1952); also see King, R. C. (Ed.) *Piping Handbook*, 5th Ed., McGraw-Hill, New York, 1967, pp. 3-26.
- 7-25. Schlichting, H., *Boundary-Layer Theory*, 6th Ed., McGraw-Hill, New York, 1968, p. 122.
- 7-26. Sovran, G., and E. D. Klomp, "Experimentally Determined Optimum Geometries for Rectilinear Diffusers with Rectangular, Conical or Annular Cross-Section," in *Fluid Mechanics of Internal Flow*, G. Sovran (Ed.), Elsevier Publishing Company, New York, 1967.
- 7-27. Reneau, L. R., et al., "Performance and Design of Straight, Two-Dimensional Diffusers," *J. Basic Eng.* **89**, 141-150 (1967).
- 7-28. Carlson, J. J., et al., "Effects of Wall Shape on Flow Regimes and Performance in Straight Two-Dimensional Diffusers," *J. Basic Eng.* **89**, 151-160 (1967).
- 7-29. Fox, R. W., and S. J. Kline, "Flow Regimes in Curved Subsonic Diffusers," *J. Basic Eng.* **84**, 303-316 (1972).
- 7-30. Stull, F. D., and H. R. Velkoff, "Flow Regimes in Two-Dimensional Ribbed Diffusers," *J. Fluids Eng.* **97**, 87-96 (1975).
- 7-31. Abdelhamid, A. N., et al., "Experimental Investigation of Unsteady Phenomena in Vaneless Radial Diffusers," ASME Paper 78-GI-23 (1978).
- 7-32. Fricke, F. R., "Periodicity in Annular Diffuser Flow," *Nucl. Sci. Eng.* **48**, 87-102 (1972).
- 7-33. Smith, C. R., and S. J. Kline, "An Experimental Investigation of the Transitory Stall Regime in Two-Dimensional Diffusers," *J. Fluids Eng.* **96**, 11-15 (1974).
- 7-34. McDonald, A. T., and R. W. Fox, "An Experimental Investigation of Incompressible Flow in Conical Diffusers," *Int. J. Mech. Sci.* **8**, 125-139 (1966).
- 7-35. Waitman, B. A., et al., "Effects of Inlet Conditions on Performance of Two-Dimensional Subsonic Diffusers," *J. Basic Eng.* **83**, 349-360 (1961). Also see Klein, A., "Review: Effects of Inlet Conditions on Conical Diffuser Performance," *J. Fluids Eng.* **103**, 250-257 (1981).
- 7-36. Moore, C. A., and S. J. Kline, "Some Effects of Vanes and of Turbulence on Two-Dimensional Wide-Angle Subsonic Diffusers," Stanford University Report NACA TN 4080, June 1958.
- 7-37. Howard, J. H. G., et al., "Performance and Flow Regimes for Annular Diffusers," ASME Paper 67-WA/FE-21, 1967; as quoted by Adenubi, S. O., "Performance and Flow Regime of Annular Diffusers with Axial Turbomachine Discharge Inlet Conditions," *J. Fluids Eng.* **98**, 236-241 (1976).
- 7-38. Wolf, S., and J. P. Johnston, "Effects of Nonuniform Inlet Velocity Profiles on Flow Regimes and Performance in Two-Dimensional Diffusers," *J. Basic Eng.* **91**, 462-474 (1969).
- 7-39. Smith, C. R., "Transitory Stall Time Scales for Plane-Wall Air Diffusers," *J. Fluids Eng.* **100**, 133-135 (1978).
- 7-40. Schachenmann, A. A., and D. O. Rockwell, "Oscillating Turbulent Flow in a Conical Diffuser," *J. Fluids Eng.* **98**, 695-701 (1976).
- 7-41. Stenning, A. H., and A. A. Schachenmann, "Oscillatory Flow Phenomena in Diffusers at Low Reynolds Numbers," *J. Fluids Eng.* **95**, 401-407 (1973).
- 7-42. Ghose, S., and S. J. Kline, "The Computation of Optimum Pressure Recovery in Two-Dimensional Diffusers," *J. Fluids Eng.* **100**, 419-426 (1978).
- 7-43. McMillan, O. J., and J. P. Johnston, "Performance of Low-Aspect-Ratio Diffusers with Fully Developed Turbulent Inlet Flows, Part II," *J. Fluids Eng.* **95**, 393-400 (1973).
- 7-44. Wirasinghe, N. E. A., and R. S. Neve, "The Prediction of Turbulent Boundary Layer Parameters in Conical Diffuser Flows," *Aeronautical Quarterly* **25**, 199-209 (1974).
- 7-45. Harsha, P. T., and H. N. Glassman, "Analysis of Turbulent Unseparated Flow in Subsonic Diffusers," *J. Fluids Eng.* **98**, 320-322 (1976).
- 7-46. Cockrell, D. J., and A. L. King, "A Review of the Literature on Subsonic Fluid Flow Through Diffusers," The British Hydro-mechanics Research Association, Report TN 902, November 1967.
- 7-47. Reneau, L. R., and J. P. Johnston, "A Performance Prediction Method for Unstalled Two-Dimensional Diffusers," *J. Basic Eng.* **89**, 643-654 (1967).
- 7-48. Miller, D. S., *Internal Flow*, BHRA Fluid Engineering, England, 1978.
- 7-49. Cockrell, D. J., and E. Markland, "A Review of Incompressible Diffuser Flow," *Aircraft Eng.* **35**, 286-292 (1963).
- 7-50. McDonald, A. T., et al., "Effects of Swirling Inlet Flow on Pressure Recovery in Conical Diffusers," *AIAA J.* **9**, 2014-2018 (1971).
- 7-51. Neve, R. S., and N. E. A. Wirasinghe, "Changes in Conical Diffuser Performance by Swirl Addition," *Aeronautical Quarterly* **29**(3), 131-143 (1978).
- 7-52. Lohmann, R. P., et al., "Swirling Flow Through Annular Diffusers with Conical Walls," *J. Fluids Eng.* **101**, 224-229 (1979).
- 7-53. Adenubi, S. O., "Performance and Flow Regime of Annular Diffusers with Axial Turbomachine Discharge Inlet Conditions," *J. Fluids Eng.* **98**, 236-242 (1976).
- 7-54. Japikse, D., and R. Pampreen, "Annular Diffuser Performance for an Automotive Gas Turbine," *J. Eng. Power* **101**, 358-372 (1979).
- 7-55. Cochran, D. L., and S. J. Kline, "Use of Short Flat Vanes for Producing Efficient Wide-Angle Two-Dimensional Subsonic Diffusers," Stanford University Report NACA TN-4309, 1958.
- 7-56. Feil, O. G., "Vane Systems for Very-Wide-Angle Subsonic Diffusers," *J. Basic Eng.* **86**, 759-764 (1964).
- 7-57. Sagi, C. J., and J. P. Johnston, "The Design and Performance of Two-Dimensional Curved Diffusers, Parts I and II," *J. Basic Eng.* **89**, 715-731 (1967).
- 7-58. Fox, R. W., and S. J. Kline, "Flow Regime in Curved Subsonic Diffusers," *J. Basic Eng.* **84**, 303-312 (1962).
- 7-59. Benedict, R. P., "Air and Water Studies on a Diffuser-Modified Flow Nozzle," *J. Fluids Eng.* **95**, 169-179 (1973).
- 7-60. Brian, T. J. S., and J. Reid, "Primary Calibrations of Critical Flow Venturi Nozzles in High-Pressure Gas," in *Flow Measure-*

- ment of Fluids*, H. H. Dijstelbergen and E. A. Spencer (Eds.), North-Holland Publishing Company, New York, 1979, pp. 55-64.
- 7-61. Halmi, D., "Metering Performance Investigation and Substantiation of the 'Universal Venturi Tube' (U.V.T.), Part 1—Hydraulic Shape and Discharge Coefficient," *J. Fluids Eng.* 96, 124-131 (1974). Also see discussion of this paper by V. P. Head, *J. Fluids Eng.* 97, 271-274 (1975).
- 7-62. Halmi, D., "Metering Performance Investigation and Substantiation of the 'Universal Venturi Tube' (U.V.T.), Part 2—Installation Effect, Compressible Flow, and Head Loss," *J. Fluids Eng.* 96, 132-138 (1974).
- 7-63. Hoffman, J. A., "Effects of Free Steam Turbulence on Diffuser Performance," *J. Fluids Eng.* 103, 385-390 (1981).